Available online at www.sciencedirect.com
SCIENCE DIRECT®
Journal of Catalysis 231 (2005) 77–91
JOURNAL OF CATALYSIS
www.elsevier.com/locate/jcat

Zeolite-catalysed liquid-phase synthesis of isopropyl *tert*-butyl ether by the addition of 2-propanol to isobutene

Montserrat Iborra, Javier Tejero *, Carles Fité, Fidel Cunill, José Felipe Izquierdo

Chemical Engineering Department, Faculty of Chemistry, University of Barcelona, Martí i Franquès, 1, 08028 Barcelona, Spain

Received 15 December 2004; revised 14 January 2005; accepted 19 January 2005

Abstract

The paper deals with the liquid-phase synthesis of isopropyl *tert*-butyl ether (IPTBE) from 2-propanol and isobutene over H-Beta, H-ZSM-5, and H-Y zeolites. The SiO_2/Al_2O_3 ratio of tested zeolites was about 25 for H-Beta, 28 for H-ZSM-5, and 6 for H-Y. Experiments were performed in a batch reactor in the temperature range of 70–90 °C at 1.6 MPa. A comparative study of the behaviour of these catalysts was made at 80 °C by with an initial alcohol-to-isobutene molar ratio ($R_{A/O}$) of 1. We optimised the activation process of the three zeolites by varying the temperature and time of calcination, thus selecting the experimental conditions of activation leading to the highest activity and selectivity. H-Beta was the most active and selective catalyst. Therefore, the kinetics of IPTBE synthesis was studied on H-Beta in the temperature range of 70–90 °C, with a $R_{A/O}$ varying from 0.7 to 2. The best kinetic model stems from a mechanism in which isobutene reacts with 2-propanol, with both adsorbed on one site, to give the ether adsorbed on one site. The apparent activation energy was estimated to be 92 ± 12 kJ mol^{-1}.

Keywords: 2-Propanol; Isobutene; IPTBE; Zeolites; H-Beta; H-Y; H-ZSM-5

1. Introduction

It is well known that *tert*-alkyl ethers such as methyl *tert*-butyl ether (MTBE), ethyl *tert*-butyl ether (ETBE), *tert*-amyl methyl ether (TAME), and isopropyl *tert*-butyl ether (IPTBE) are good components for reformulated gasolines [1]. Today, since MTBE is soluble enough in water, it is suspected of contaminating surface water in the case of gasoline reservoir kinks or even being partially dissolved by rainwater from gasoline evaporative emissions. ETBE, TAME, and IPTBE can be used more confidently in current gasolines since they are less soluble in water. IPTBE, the most unfamiliar of the three, has the triple advantages of (i) highest octane blending values, (ii) lowest oxygen content, and (iii) low vapour pressure. Moreover, IPTBE is a completely refinery-based ether because the oxygen source is water, and its production is certainly interesting if it is combined with that of diisopropyl ether (DIPE) [2]. On the other hand, IPTBE has a lower volatility and water solubility than diethyl ether and DIPE, which accounts for its potential use as a solvent in the chemical and pharmaceutical industries. Still, right now interest in IPTBE is only academic, and thus only a few papers can be found in the literature concerning the liquid-phase etherification of isobutene with 2-propanol [3–8].

As is usually done in industrial processes of synthesis of isobutene-derived *tert*-alkyl ethers (MTBE, ETBE), IPTBE is obtained by the acid-catalysed addition of the alcohol (2-propanol) to isobutene. The reaction takes place on ion-exchange resins at mild temperatures (50–90 °C) and at a pressure of 1.4–1.8 MPa to maintain the reaction medium in the liquid phase

$$(CH_3)_2CHOH + (CH_3)_2C{=}CH_2 \rightleftharpoons (CH_3)_3C{-}O{-}CH(CH_3)_2.$$

* Corresponding author. Fax: +34 93 402 1291.
E-mail address: tejero@angel.qui.ub.es (J. Tejero).

0021-9517/$ – see front matter
doi:10.1016/j.jcat.2005.01.027

The reaction is less favoured thermodynamically than the related reactions of MTBE and ETBE syntheses. Because of the low isobutene equilibrium conversion, side reactions can easily take place, decreasing the selectivity for IPTBE. Side reactions involved are [3]:

1. Isobutene dimerisation to 2,4,4-trimethyl-1-pentene (TMP-1) and 2,4,4-trimethyl-2-pentene (TMP-2) and the isomerisation reaction of isobutene dimers

$$2(CH_3)_2C{=}CH_2 \rightleftharpoons CH_2{=}C(CH_3)CH_2C(CH_3)_3 \quad \text{[TMP-1]},$$

$$2(CH_3)_2C{=}CH_2 \rightleftharpoons (CH_3)_2C{=}CHC(CH_3)_3 \quad \text{[TMP-2]},$$

$$CH_2{=}C(CH_3)CH_2C(CH_3)_3 \rightleftharpoons (CH_3)_2C{=}CHC(CH_3)_3;$$

2. Isopropanol dehydration to diisopropyl ether

$$2(CH_3)_2CHOH \rightleftharpoons H_2O + (CH_3)_2CH{-}O{-}CH(CH_3)_2;$$

3. Isopropanol dehydration to propene

$$(CH_3)_2CHOH \rightleftharpoons H_2O + CH_3CH{=}CH_2;$$

4. Isobutene hydration to *tert*-butyl alcohol (TBA)

$$(CH_3)_2C{=}CH_2 + H_2O \rightleftharpoons (CH_3)_3COH;$$

5. Decomposition of IPTBE to propene and TBA

$$(CH_3)_3C{-}O{-}CH(CH_3)_2 \rightleftharpoons CH_3CH{=}CH_2 + (CH_3)_3OH;$$

6. Etherification of 1-butene and 2-butene, with 2-propanol forming isopropyl *sec*-butyl ether [IPSBE] (if the isobutene source is a C_4 cut)

$$(CH_3)_2CHOH + CH_3CH{=}CHCH_3 \rightleftharpoons CH_3CH_2C(CH_3)HOCH(CH_3)_2,$$

$$(CH_3)_2CHOH + CH_2{=}CHCH_2CH_3 \rightleftharpoons CH_3CH_2C(CH_3)HOCH(CH_3)_2.$$

By-products are undesirable since they could create difficulties in separation units and the later use of unreacted C_4 streams that would concentrate TBA and water. The presence of TMP-1, TMP-2, and DIPE in the IPTBE product does not cause problems for gasoline blending, since all of these compounds have a high octane number. However, isobutene could oligomerise to give polymers that decrease the catalyst activity by overlaying its surface and lowering the amount of accessible acid sites. As IPSBE has a more linear structure than IPTBE, it can be assumed that IPSBE has a lower octane number than IPTBE, and it would reduce the octane number of the IPTBE product.

Despite the fact that liquid-phase etherification of isobutene with alcohol is conducted industrially on acidic ion-exchange resins, zeolites have frequently been proposed as catalysts for these reactions. Compared to ion exchangers, zeolites are thermally stable, give no acid effluent on overheating, and are less sensitive to the alcohol-to-isobutene molar ratio [9]. Generally, zeolites do not appear to be highly active for the etherification of olefins, probably because of their smaller number of acid sites. However, experimental studies on the gas-phase synthesis of MTBE and ETBE by the addition of methanol and ethanol, respectively, to isobutene on a series of zeolites show that H-Beta is as active as Amberlyst-15, and the activity of the usual zeolites decreases as follows: H-Beta > H-Y > H-ZSM-5 [10,11].

As for the liquid-phase synthesis of MTBE, Collignon et al. [12] studied the reaction on Amberlyst-15, H-Beta, and H-Y, and their results supported their previous studies in the gas phase. The liquid-phase syntheses of MTBE [13–16] and ETBE [17] were also studied on H-ZSM-5. As a rule, it was found that zeolites are more selective for ethers than is Amberlyst-15 in a wide range of alcohol/isobutene molar ratios.

In this paper, the liquid-phase synthesis of IPTBE from isobutene and 2-propanol is studied over H-Beta and H-Y. These large-pore zeolites are expected to be suitable since the IPTBE molecule is bulkier than MTBE. For the sake of comparison, an H-ZSM-5 zeolite is used as well. The aim of the paper is first to compare their catalytic behaviours and second to study the kinetics of the reaction on the most active and selective catalyst.

2. Experimental

2.1. Materials

2-Propanol (> 99.9%, water content < 0.01%) was obtained from ROMIL Chemical Ltd. (Shepshed, England) and stored over 3-Å molecular sieves (Fluka, Buchs, Switzerland). Isobutene (> 99%) was supplied by Air Liquide (Barcelona, Spain) and used without further purification. We prepared IPTBE in our laboratory by reacting 2-propanol and isobutene on Amberlyst-15, which we purified by extracting the alcohol with water and further distillation up to 99.8% purity (GC) and identified by MS and NMR. *tert*-Butyl alcohol (> 99%, Merck-Schuchardt, Hohenbrunn, Germany), 2,4,4-trimethyl-1-pentene (> 98%, Fluka), 2,4,4-trimethyl-2-pentene (> 98%, Fluka), and DIPE (> 99%, Fluka) were used to prepare standards for analysis.

2.2. Catalysts

The catalysts used were H-ZSM-5 (Degussa Ibérica, Barcelona, Spain), H-Y (Aldrich, USA), and H-Beta (Südchemie, Bruckmühl-Heufeld, Germany). Their physical and textural properties are listed in Table 1.

2.3. Characterisation techniques

Zeolites were used as a powder. They consisted of a collection of aggregates of small crystallites ranging from 0.7 to 40 μm; the mean size was between 4 and 8 μm. The distribution of aggregate sizes was determined in water and in 1-pentanol by a laser technique with a Microtrack

Table 1
Physical and structural properties of zeolites

	H-Beta	H-Y	H-ZSM-5
SiO_2/Al_2O_3	25.1	5.7	27.9
Brønsted acid site concentration (mm g^{-1})	1.2	4.2	1.12
Mean particle size (μm)	8.1	4.4	3.9
Mean crystal size[a] (μm)	0.2–0.3	0.6–0.7	0.8–1.2
Mean crystal size[b] (μm)	0.1–0.3	0.5–0.8	1–1.4
Skeletal density, ρ_s (g cm^{-3})	2.237	2.026	2.083
BET surface area, S_g (m^2 g^{-1})	594	770	419
Pore volume, V_g (cm^3 g^{-1})	0.724	0.525	0.241
External surface area, S_{ext}[c] (m^2 g^{-1})	246	108	28
Micropore volume, V_μ[c] (cm^3 g^{-1})	0.150	0.274	0.168
Mesopore surface, S_{meso}[d] (m^2 g^{-1})	232	81	34
Mesopore volume, V_{meso}[d] (cm^3 g^{-1})	0.626	0.147	0.053
Mean mesopore diameter, $\bar{d}_{pore}$ (nm)	10.8	7.3	6.2
Micropore diameter[e] (nm)	0.65 × 0.56; 0.75 × 0.57	0.74	0.53 × 0.56; 0.54 × 0.55
Cage diameter[e] (nm)		1.15	

[a] From TEM micrographs.
[b] From SEM micrographs.
[c] Calculated by the *t*-method of Lippens–de Boer [20].
[d] Calculated according to Ref. [21].
[e] Values obtained from molecular models [22].

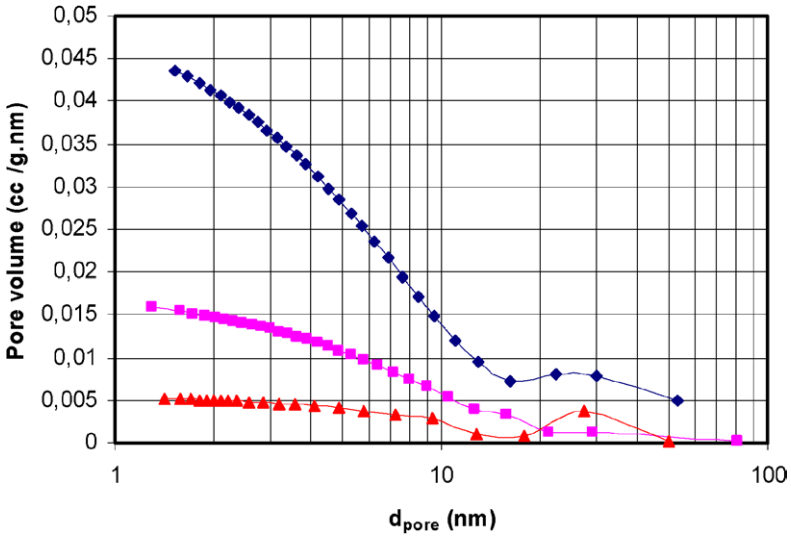

Fig. 1. Pore size distribution curves of H-Beta (◆), H-Y (■), and H-ZSM-5 (▲).

SRA analyser. Transmission electron micrographs (Hitachi H600-AB) showed that zeolite powders were composed of small crystallites typically in the range of 0.1–1.5 μm. Scanning electron micrographs (Hitachi, S-2300) backed up this fact. As can be seen from Table 1, the crystal sizes of tested zeolites varied in the pattern H-Beta < H-Y < H-ZSM-5.

SiO_2/Al_2O_3 molar ratios were measured by X-ray fluorescence (PW1400, Philips; detector: LiF crystal; excitation source: Rh). We estimated acid site densities by assuming one Brønsted acid site per lattice Al free of residual cations such as Na^+ [18].

Textural properties were obtained from N_2 adsorption–desorption isotherms recorded at 77 K with an Accusorb ASAP 2020 sorptometer (Micromeritics, Norcross, GA) after the samples were outgassed at 500 °C for 4 h. BET surface areas were measured with the use of recorded data at $0.05 \leqslant P/P_0 \leqslant 0.25$. Pore volume, V_g, was estimated from the volume of N_2 adsorbed at a relative pressure of 0.99. External surface areas, S_{ext}, and micropore volumes, V_μ, were computed by the *t*-method of Lippens–de Boer [19,20]. Pore size distributions in the meso- and macropore range ($2 \leqslant d_{pore} \leqslant 50$ nm) were calculated by the Barret–Joyner–Halenda method based on the Kelvin equation [21]. As Table 1 shows, zeolites have a very distinct surface area and pore volume in this range. It is should be noted that the estimates of S_{ext} and S_{meso} agree quite well, showing that the extra-crystalline area of H-Beta is larger than that of H-ZSM-5 by an order of magnitude, whereas that of H-Y is intermediate. As Fig. 1 shows, distinct distribution curves were observed: H-Beta has pores in the range of 2–50 nm;

H-Y has practically no pores higher than 10 nm; whereas H-ZSM-5 has almost no mesopores. An estimation of mesopore diameter was made by assuming the cylindrical pore model. Finally, skeletal density, ρ_s, was measured by helium displacement with an Accupyc 1330 (Micromeritics).

2.4. Apparatus

The experiments were carried out in a stainless-steel jacketed 300-cc autoclave (Autoclave Engineers, USA) operating in batch mode. The reaction medium was stirred at 500 rpm by a magnetic-drive turbine. Thermostatted water flowing through the jacket controlled the temperature to within ±0.2 K. To maintain the reacting mixture in the liquid phase over the whole temperature range, the pressure was set at 1.6 MPa by means of N_2. One of the outlets of the reactor was connected directly to a liquid sampling valve (VALCO 4-CL4WE), which injected 0.2 µl of pressurised liquid into a GLC HP 5890A equipped with FID. More detailed information about the setup can be found elsewhere [23].

2.5. Analysis

A 50 m × 0.2 mm × 0.5 µm (length × ID × film thickness) methyl silicone column (PONA-HP 19091S-001) was used to separate and determine 2-propanol, isobutene, IPTBE, TBA, DIPE, TMP-1, and TMP-2. The PONA column was temperature programmed with a 7-min initial hold at 313 K, followed by a 20 K min^{-1} ramp up to 433 K, and held for 15 min. Helium (Air Liquide, Barcelona, Spain) with a minimum purity of 99.998% was used as the carrier gas. The carrier gas flow rate was 30 ml min^{-1}.

2.6. Procedure

Zeolites were activated by calcination under an air stream in a muffle furnace. Calcined zeolite samples were kept at vacuum (10^{-4} mm Hg) overnight.

A calculated amount of 2-propanol and the calcined zeolite were first carefully charged into the reactor to minimise the possible rehydration of the catalyst. After looking for leaks, we heated the reactor to the target temperature. Once that temperature was reached, the corresponding amount of liquid isobutene, given by the desired initial alcohol/olefin molar ratio, $R_{A/O}$, was measured volumetrically at 0.8 MPa in a pressurised burette and fed to the reactor with nitrogen as the carrier. Then the stirrer was switched on at 500 rpm, and the reactor pressure was set at 1.6 MPa. The introduction of the isobutene into the reactor was taken as the starting point of the reaction. To follow the concentration variation of chemicals with time, we periodically removed and analysed liquid samples.

3. Results and discussion

3.1. Selection of the best catalyst

Zeolites were tested at 80 °C and $R_{A/O} \approx 1$ to select the most active and selective catalyst. Previous runs showed that chemical equilibrium was reached within 3–5 h with 0.5 g of H-Beta or 2 g of H-Y, but it took 9 h with 17 g of H-ZSM-5. Their catalytic activities are therefore very different. Fig. 2 shows how the liquid-phase composition changes with time in a typical experiment on H-ZSM-5. As can be seen, moles of isobutene and 2-propanol lessen continuously, whereas those of IPTBE increase, until chemical equilibrium is reached. The by-products detected were TMP-1, TMP-2, DIPE, and TBA.

The initial reaction rate of IPTBE synthesis, r^0_{IPTBE}, was used to compare zeolite activities. It was measured from the slope of the curve of IPTBE moles formed versus reaction time at $t = 0$ according to the expression

$$r^0_{IPTBE} = \frac{1}{W}\left(\frac{dn_{IPTBE}}{dt}\right)_{t=0}. \quad (1)$$

To compare the selectivities of zeolites meaningfully, they were studied at equilibrium. The selectivity of IPTBE

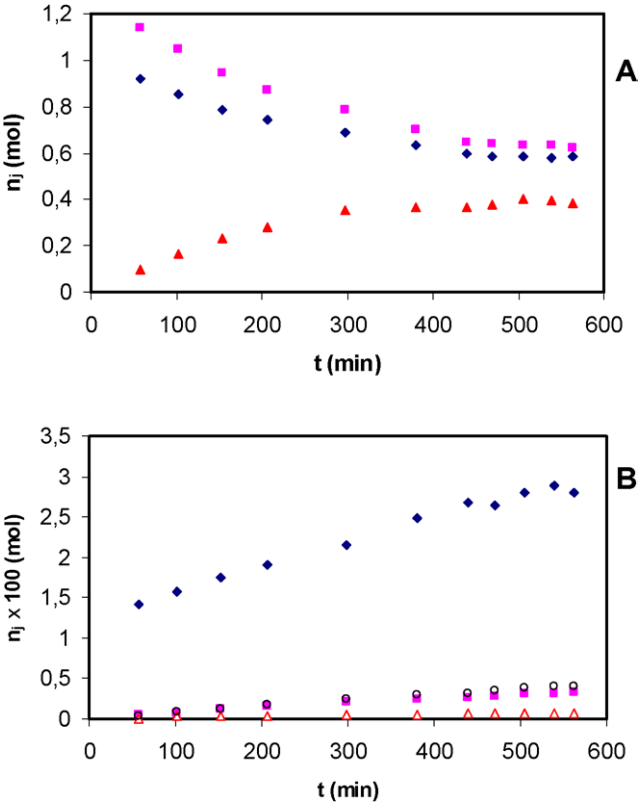

Fig. 2. Mole of 2-propanol, isobutene, IPTBE and by-products vs. time at 80 °C and $R_{A/O} = 1$ over 17 g of H-ZSM-5 activated at 200 °C for 3 h. (A) IB (◆), IPA (■), and IPTBE (▲). (B) TBA (◆), TMP-1 (■), TMP-2 (▲), and DIPE (○).

Table 2
Activation conditions for H-Beta, H-Y and H-ZSM-5 as catalysts for the synthesis of *tert*-alkyl ethers such as MTBE and ETBE quoted in literature

Catalyst	Activation conditions	Reference
H-Beta	400 °C for 3 h under He stream	[10,12]
	538 °C for 3 h in air	[13]
H-Y	400 °C for 3 h under He stream	[10,12]
	120 °C for 12 h in air	[30]
	200 °C for 2 h in N_2	[35]
	Ramp of 2 °C/min from room temperature to 400 °C under He stream; 400 °C is held for 2 h	[28,30]
	Id, but final temperature of 400 °C is held for 12 h	[29,33,34]
	Ramp of 2 °C/min from room temperature to 180 °C, held for 2 h	[32]
H-ZSM-5	400 °C for 3 h under He stream	[10,12]
	538 °C for 3 h in air	[13]
	500 °C for 5 h under N_2 stream	[14]
	500 °C for 4 h under air stream	[26,27]
	Ramp of 2 °C/min from room temperature to 400 °C under He stream; 400 °C is held for 12 h	[29,33,34]
	Id, but final temperature of 400 °C is held for 2 h	[31]
	Ramp of 2 °C/min from room temperature to 180 °C, held for 2 h	[32]

with respect to isobutene (IB) was defined as [24,25]

$$S_{\mathrm{IB}}^{\mathrm{IPTBE}} = \frac{\text{moles of IB reacted to form IPTBE}}{\text{moles of IB reacted}}. \quad (2)$$

To assess quantitatively the presence of by-products, the selectivity of a by-product relative to IPTBE was defined as follows:

$$S_{\mathrm{IPTBE}}^{j} = \frac{\text{moles of compound } j \text{ formed}}{\text{moles of IPTBE generated}}. \quad (3)$$

Replicated experiments allowed us to establish that estimates of the initial reaction rate were accurate within ±5%, and IB conversion and selectivities at equilibrium within ±3%.

Some activation procedures for zeolites are customary (Table 2) and consist of heating at constant temperature, or with a temperature ramp, under a stream of He, N_2, or air. The upper temperature is maintained for 2 to 12 h to ensure that water removal is complete. In our case, zeolites were heated at constant temperature under an air stream, and the time and temperature of activation were optimised to properly compare their catalytic behaviours. An experimental series with zeolites heated at 100–550 °C for 3 h was carried out first. From r^0_{IPTBE} measurements, Fig. 3A shows that, within the limits of the experimental error, there is an optimal range of calcination temperature, T_c, for each zeolite: $405 \leqslant T_c \leqslant 470$ °C for H-Beta, $450 \leqslant T_c \leqslant 550$ °C for H-Y, and $200 \leqslant T_c \leqslant 300$ °C for H-ZSM-5.

Water is removed in the calcination process, and Brønsted acid centres become active to catalyse IPTBE synthesis. But, at high T_c, Brønsted centres change into Lewis centres, and at $T_c > 700$ °C zeolites decompose [36]. Since thermal decomposition is not likely in the T_c range explored, the optimal T_c ranges found correspond to temperatures where the highest number of Brønsted acid sites is available. It is worth noting that the optimal activation range for H-Y is in good agreement with that quoted by Ward for ammonium Y zeolites (400–600 °C) [37].

Figs. 3B–D show isobutene conversion, X_{IB}, and selectivity for IPTBE and IPTBE yield, Y_{IPTBE}, at equilibrium. X_{IB} on H-Beta and H-Y is higher than on H-ZSM-5; but H-Y is the most selective for IPTBE. However, Y_{IPTBE} (defined as mole of ether formed per mole of isobutene fed) shows that both H-Y and H-Beta give higher amounts of IPTBE at equilibrium.

As for by-products, TBA, TMP-1, and TMP-2 were detected on all of the zeolites. TBA is formed by reaction of IB with odd water after the activation process. The higher T_c is, the less water remains after calcination; therefore the amount of TBA decreases with increasing T_c, as seen on H-ZSM-5 (Fig. 3E), but TBA amounts are random on H-Beta and H-Y. On the other hand, as Figs. 3F and H show, the amounts of TMP-1 and TMP-2 increase with T_c on the three zeolites. It should be noted that the amount of TMP-1 is higher than the amount of TMP-2 by four times on H-ZSM-5, which is the same distribution of dimers as found with mineral acids [38]. Over H-Beta and H-Y, the amount of TMP-1 is far higher than the amount of TMP-2, particularly on H-Beta. Finally, DIPE was detected only on H-Y and H-ZSM-5, but the DIPE amount was very low.

Then we tested zeolites calcined at the central temperature of the optimal range (H-Beta, 440 °C; H-Y, 500 °C; H-ZSM-5, 250 °C) but with varying drying time, t_c, from 2 to 4 h. As can be seen in Table 3, initial reaction rates and selectivity data do not change with drying time, within the limits of the experimental error, on each zeolite.

As Table 3 shows, H-Beta is more active than H-Y and, in particular, H-ZSM-5. This is consistent with the literature, since Collignon et al. reported that the larger S_{ext} was, the higher was the activity of zeolites in yielding MTBE [10,12]. Still, the reaction rate could also be influenced by the distinct number of acid sites. To make sure of this, a fit of initial reaction rates by a general potential model, $r^0_{\mathrm{IPTBE}} = k[\mathrm{H}^+]^{\alpha} S_{\mathrm{ext}}^{\beta}$, was performed, in which we obtained $\alpha = 2.44$ and $\beta = 0.176$. Thus, the reaction rate of IPTBE synthesis depends chiefly on the external surface

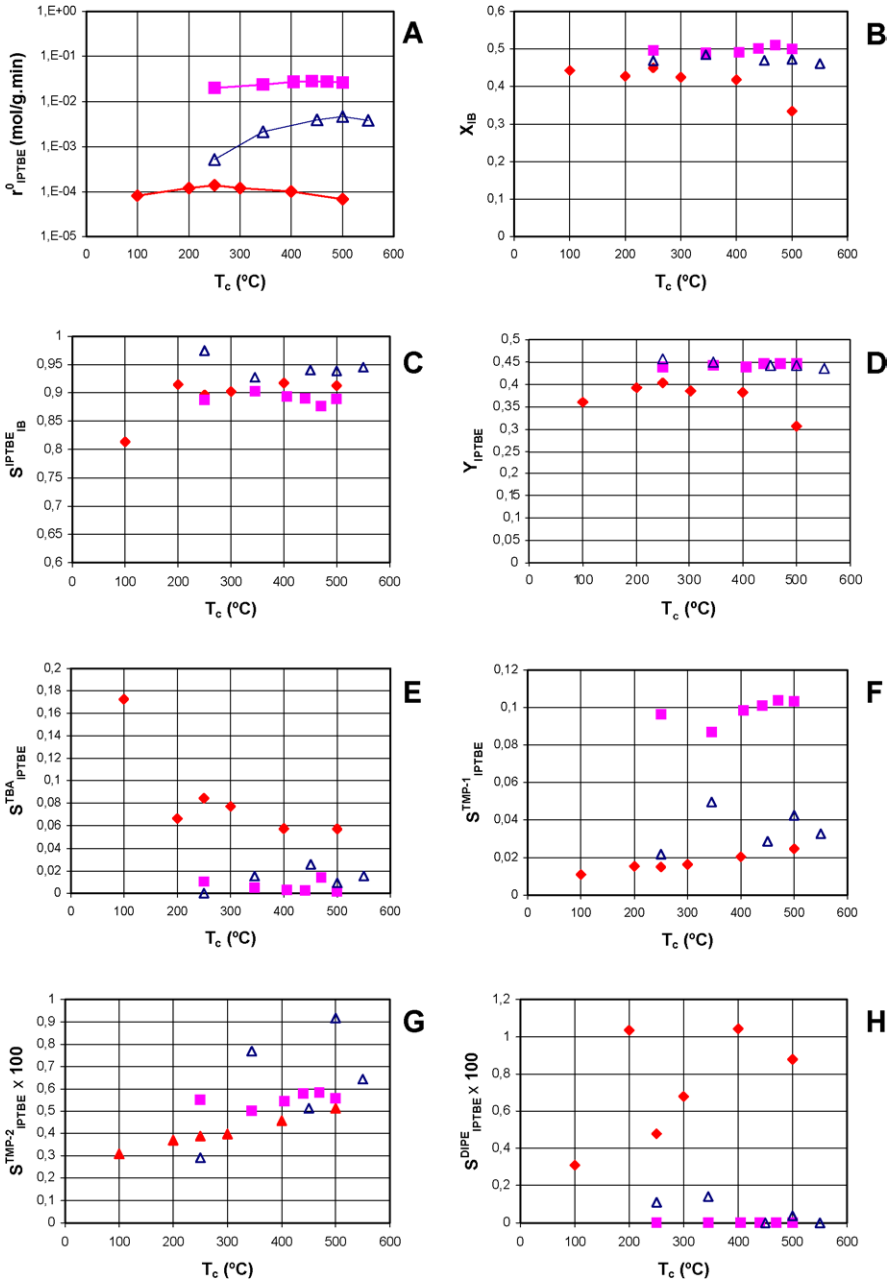

Fig. 3. Catalytic behaviour of H-Beta, H-Y and H-ZSM-5 at 80 °C and $R_{A/O} = 1$ as a function of T_c at $t_c = 3$ h. (A) Initial reaction rate; (B) IB conversion; (C) selectivity to IPTBE; (D) IPTBE yield; (E) selectivity to TBA relative to IPTBE; (F) selectivity to TMP-1 relative to IPTBE; (G) selectivity to TMP-2 relative to IPTBE; (H) selectivity to DIPE relative to IPTBE (◆, H-ZSM-5; ■, H-Beta; △, H-Y).

of the zeolites. However, the dependence of r^0_{IPTBE} on S_{ext} is stronger than the linear one reported by Collignon et al. for H-Beta zeolites [12]. Accordingly, the reaction rate on H-ZSM-5 and H-Y is much lower than what could be expected from the S_{ext} values (Fig. 4). It could be explained by the possibility that micropores contribute to some extent to the reaction, especially in H-ZSM-5, which has the smallest S_{ext}, as the by-product distribution suggests. The odd water amount is relatively high after activation, and, as a result, TBA is the main by-product. Furthermore, the fact that the TMP-1/TMP-2 molar ratio is about the same as the one found with soluble catalyst agrees well with the common picture that catalysis in H-ZSM-5 pores is homogeneous-like [37]. On zeolites of larger S_{ext}, the selectivity changes when the contribution of the micropores decreases. Thus, TBA and IB dimers appear in similar amounts on H-Y, but TMP-1 is by far the main by-product on H-Beta. From a kinetic standpoint, reaction within micropores is seriously limited by conformational diffusion, since the molecular sizes of IPTBE and the by-products are close to the micropore width, as Table 4 shows, if the random coil diameter, δ, is assumed to be representative of the molecular size [39].

Table 3
Initial reaction rate, isobutene conversion and selectivity at equilibrium ($T = 80\,^{\circ}C$, $R_{A/O} = 1$) as a function of calcination time

T_c (°C)	t_c (h)	r^0_{IPTBE} (mol g^{-1} min^{-1})	X_{IB}	S^{IPTBE}_{IB}	S^{TBA}_{IPTBE}	$S^{TMP\text{-}1}_{IPTBE}$	$S^{TMP\text{-}2}_{IPTBE}$	S^{DIPE}_{IPTBE}
				H-ZSM-5				
250	2	1.38×10^{-4}	0.449	0.904	0.083	0.0089	0.0022	0.011
	3	1.38×10^{-4}	0.449	0.897	0.094	0.0084	0.0022	0.0048
	4	1.40×10^{-4}	0.449	0.899	0.089	0.0094	0.0022	0.0075
				H-Beta				
440	2	2.79×10^{-2}	0.504	0.893	0.0053	0.054	0.0031	0
	3	2.77×10^{-2}	0.501	0.891	0.0030	0.057	0.0033	0
	4	2.79×10^{-2}	0.502	0.886	0.0052	0.057	0.0032	0
				H-Y				
500	2	4.59×10^{-3}	0.471	0.942	0.010	0.021	0.0047	0.0003
	3	4.68×10^{-3}	0.472	0.939	0.010	0.022	0.0049	0.0004
	4	4.41×10^{-3}	0.471	0.942	0.012	0.020	0.0043	0.0002

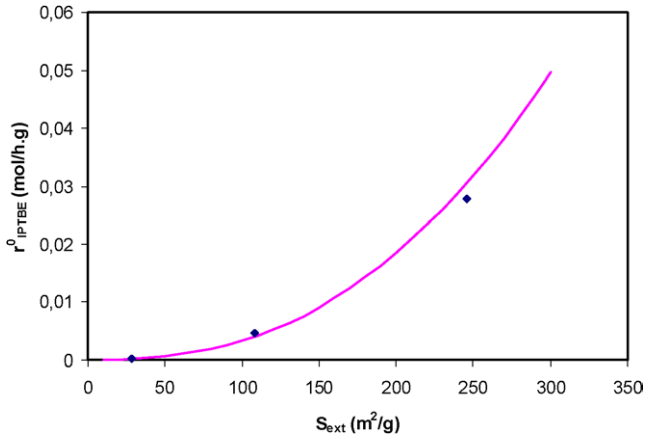

Fig. 4. Initial reaction rate of IPTBE synthesis at 80 °C and $R_{A/O} = 1$ vs. external surface (H-Y, ◆; H-ZSM-5, ■; H-Beta, ▲).

Table 4
Random coil diameter of 2-propanol, isobutene, IPTBE and by-products, computed by $\delta = 0.2457\overline{M}^{0.5882}$ (δ, random coil diameter; $\overline{M}$, molecular weight of compound) [39]

Compound	$\overline{M}$ (g mol^{-1})	δ (Å)
Water	18.016	1.346
Isobutene	56.108	2.625
2-Propanol	60.097	2.734
TBA	74.124	3.093
IPTBE	116.205	4.029
TMP-1, TMP-2	112.216	3.947
DIPE	102.178	3.735

The nature and quantity of active sites should be considered as well. In the adsorption of methanol on H-ZSM-5, H-Y, and H-Beta, significant differences were observed by Hunger and Horvath [40]. On H-ZSM-5 and H-Y, methanol adsorbs preferably on SiOHAl groups and forms adsorbate complexes consisting of a maximum of four alcohol molecules per zeolite OH group. On H-Beta, a significant adsorption on SiOH groups and an adsorption capacity of up to 7.5 methanol molecules per zeolite OH group were found. The alcohol molecules, which are part of the adsorbate complexes in H-Beta, are weakly hydrogen-bonded and represent, therefore, a reservoir of activated reactant molecules in those heterogeneously catalysed reactions that use methanol as an educt molecule. Such an interesting property of H-Beta could explain the reaction rates for IPTBE synthesis found in this work, if we assume that the rates of adsorption of 2-propanol and methanol on H-ZSM-5, H-Y, and H-Beta are alike.

It is interesting to compare the catalytic behaviours of H-Beta, H-Y, and H-ZSM-5 with that of macroporous resins commonly used in the industrial processes of the synthesis of *tert*-alkyl ethers, that is, Amberlyst 15 and 35. As Table 5 shows, despite the fact that H-Beta has a lower acid capacity, the initial reaction rate is comparable to that of resins; this can be explained by the higher acid strength of acid sites on zeolites [41]. Zeolites are less selective for IPTBE, but the distributions of by-products on H-Beta and ion exchangers are similar; TMP-1 is the main by-product. Nonetheless, since selectivity for IPTBE is only a bit less, H-Beta can be looked at as an option for obtaining IPTBE industrially. The higher quantities of isobutene dimer that would be produced do not pose any problems, since its octane number is close to that of IPTBE. Therefore, the study of IPTBE synthesis on H-Beta was undertaken.

3.2. Experiments on H-Beta

Experiments were performed at 69.2, 79.4, and 89.5 °C at a $R_{A/O}$ of 0.7, 1, and 2. A catalyst mass of 0.37–0.43 g of H-Beta (catalyst loading < 1%), activated at 440 °C for 3 h, was used. Chemical equilibrium was reached within 2 to 2.5 h at 89.5 °C; 4 h was required at 79.4 °C and about 8 h at 69.2 °C. As Fig. 5A shows, the initial reaction rate decreases as $R_{A/O}$ increases, that is, when the initial 2-propanol concentration increases. Figs. 5B–D show that X_{IB} and selectivity for IPTBE at equilibrium increase with $R_{A/O}$ and temperature and, as a result, Y_{IPTBE} increases, as expected. The formation of IB dimers rises with temperature and with decreasing $R_{A/O}$ (Figs. 5E and F), whereas the amounts of

Table 5
Initial reaction rate, IB conversion, and selectivity at equilibrium ($T = 80\,^{\circ}C$; $R_{A/O} = 1$). Zeolites are calcined at optimal T_c and t_c, and resins dried at 110 °C under vacuum for 3 h [42]

Catalyst	Acid site concentration (mm g^{-1})	r^0_{IPTBE} (mol g^{-1} min^{-1})	X_{IB}	S^{IPTBE}_{IB}	S^{TBA}_{IPTBE}	$S^{TMP\text{-}1}_{IPTBE}$	$S^{TMP\text{-}2}_{IPTBE}$	S^{DIPE}_{IPTBE}
Amberlyst-35	5.3 [a]	4.7×10^{-2}	0.496	0.935	0.0061	0.015	0.0056	0.0022
Amberlyst-15	4.8 [a]	2.1×10^{-2}	0.488	0.962	0.0034	0.013	0.0051	0.0013
H-Beta	1.2	2.79×10^{-2}	0.501	0.891	0.0030	0.057	0.0033	0
H-Y	4.2	4.68×10^{-3}	0.472	0.939	0.010	0.022	0.0049	0.0004
H-ZSM-5	1.12	1.38×10^{-4}	0.449	0.897	0.094	0.0084	0.0022	0.0048

[a] From Ref. [8].

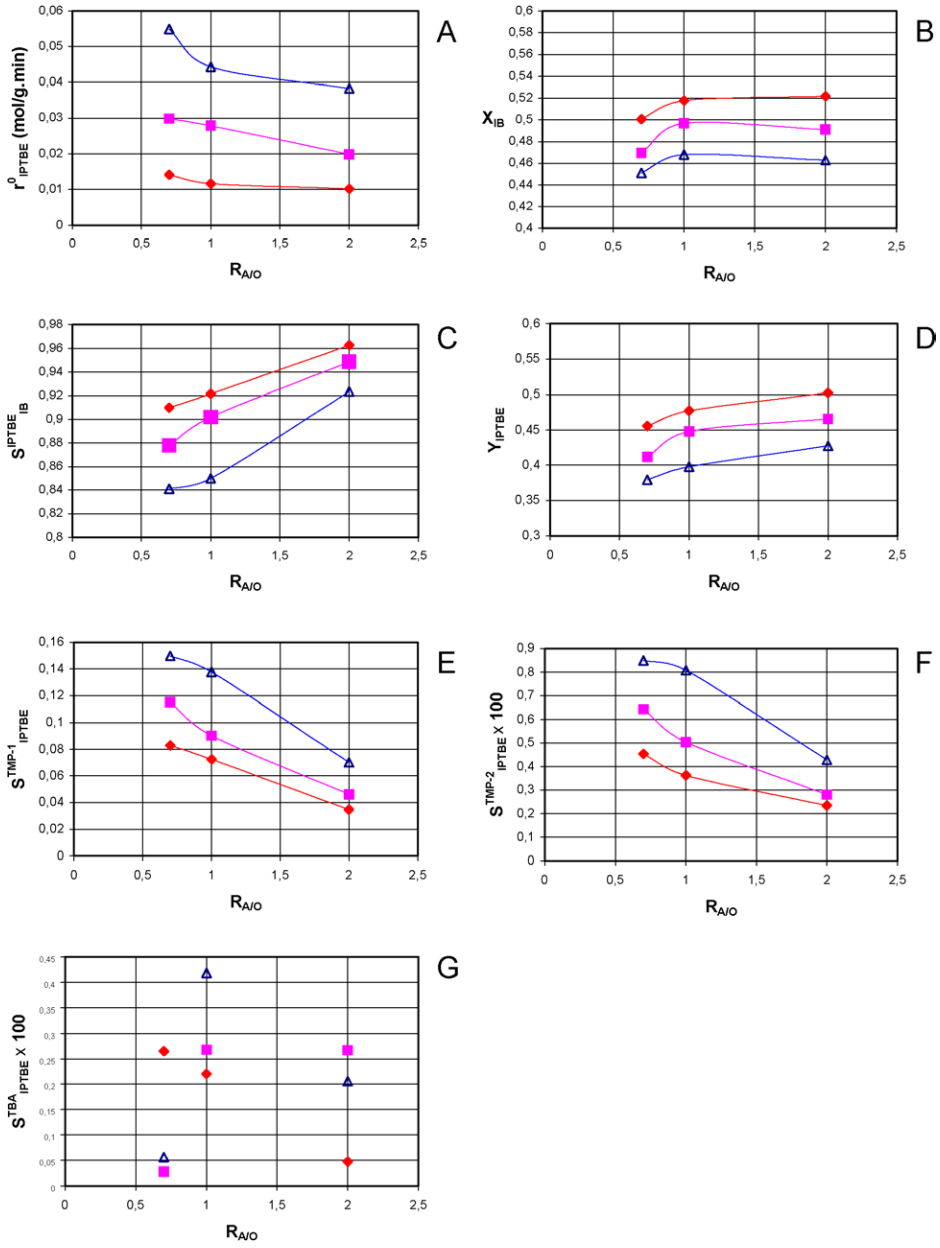

Fig. 5. Catalytic behaviour of H-Beta as a function of $R_{A/O}$: (A) initial reaction rate; (B) IB conversion; (C) selectivity to IPTBE; (D) IPTBE yield; (E) selectivity to TMP-1 relative to IPTBE; (F) selectivity to TMP-2 relative to IPTBE; (G) selectivity to TBA relative to IPTBE (69.2 °C, ◆; 79.4 °C, ■; 89.5 °C, △).

TBA are random (Fig. 5G), since it forms from odd water over the catalyst. DIPE was detected only at 89.5 °C.

3.3. Kinetic study based on initial reaction rates

In a previous study of IPTBE synthesis on Amberlyst-35, performed in the same setup, it was found that at 500 rpm, external mass transfer had no effect on the reaction rate on resin beads with diameters between 0.08 and 0.1 mm [43]. The external mass transfer rate depends on particle size and on the reaction rate itself. Since resin beads are 10 times larger than zeolite beads, and reaction rates on H-Beta are a bit less than on Amberlyst-35 (Table 5), we can conclude that the reaction takes place on H-Beta free of external mass transfer effects.

Resistance to intraparticle diffusion is reduced to negligible proportions with the use of sufficiently small catalyst particles. To determine whether reaction rates are influenced by intraparticle diffusion, the experiment performed under the most adverse conditions, giving the highest reaction rate, is examined. The appropriate run is that performed at 89.5 °C and $R_{A/O} = 0.7$. The criterion for observing chemically controlled reaction rates is that the Weisz–Prater modulus, in terms of measurable quantities, should be [44]

$$\Phi = \frac{L_e^2 r_{IPTBE} \rho_P}{D_{e,IPA} c_{IPA,S}} \ll 1, \tag{4}$$

where L_e is the effective diffusion-path-length parameter (a third of the radius for spherical beads), r_{IPTBE} is the reaction rate of IPTBE synthesis, ρ_P is the particle density ($= \rho_S(1-\theta)$; θ = catalyst porosity), $D_{e,IPA}$ is the effective diffusivity of the limiting compound (at $R_{A/O} = 0.7$, 2-propanol), and $c_{IPA,S}$ is the 2-propanol concentration at the external surface. As can be seen in Table 6, the observed reaction rates are not influenced by diffusion in mesopores; however, despite the fact that H-Beta crystallites are very small (see Table 1), resistance to diffusion in micropores cannot be wholly discarded, since conformational diffusion is far slower than diffusion in mesopores. Fortunately, as discussed above, IPTBE synthesis occurs chiefly at the mesopore surface.

Table 6
Application of Weisz–Prater criterion to test resistance to intra-particle and intra-crystallite diffusion

Parameter	Intra-particle diffusion	Intra-crystalline diffusion
L_e (m)	1.4×10^{-6}	5×10^{-8}
$r = r^0_{IPTBE}$ (mol g^{-1} min^{-1})	0.0549	0.0549
ρ_P (g cm^{-3})	0.854	0.854
$D_{e,IPA}$ (m^2 s^{-1})	2.4×10^{-9} [a]	10^{-10}–10^{-18} [b]
$C_{IPA,S}$ (mol l^{-1})	4.8	4.8
Φ	1.33×10^{-4}	5×10^{-6}–550

[a] Estimated by the procedure outlined by Taylor and Krishna [45].
[b] Range for conformational diffusivity according to Weisz [46].

To perform the kinetic study, it was assumed that the reaction takes place either by a Rideal–Eley mechanism (ER) in which isobutene from solution reacts with 2-propanol adsorbed on an active centre,

$$\text{IPA} + \sigma \rightleftharpoons \text{IPA}\cdot\sigma,$$
$$\text{IPA}\cdot\sigma + \text{IB} \rightleftharpoons \text{IPTBE}\cdot\sigma,$$
$$\text{IPTBE}\cdot\sigma \rightleftharpoons \text{IPTBE} + \sigma;$$

or by a Langmuir–Hinshelwood–Hougen–Watson (LHHW) mechanism in which isobutene and 2-propanol, both adsorbed on an active centre, react to give IPTBE:

$$\text{IPA} + \sigma \rightleftharpoons \text{IPA}\cdot\sigma,$$
$$\text{IB} + \sigma \rightleftharpoons \text{IB}\cdot\sigma,$$
$$\text{IPA}\cdot\sigma + \text{IB}\cdot\sigma \rightleftharpoons \text{IPTBE}\cdot\sigma + \sigma,$$
$$\text{IPTBE}\cdot\sigma \rightleftharpoons \text{IPTBE} + \sigma.$$

In addition, a LHHW mechanism, wherein an additional active centre is needed in the surface reaction step, was considered as follows:

$$\text{IPA} + \sigma \rightleftharpoons \text{IPA}\cdot\sigma,$$
$$\text{IB} + \sigma \rightleftharpoons \text{IB}\cdot\sigma,$$
$$\text{IPA}\cdot\sigma + \text{IB}\cdot\sigma + \sigma \rightleftharpoons \text{IPTBE}\cdot\sigma + 2\sigma,$$
$$\text{IPTBE}\cdot\sigma \rightleftharpoons \text{IPTBE} + \sigma.$$

The last mechanism was considered to compare with resins, since in kinetic studies over Amberlyst-15, Amberlyst-35, and Bayer K-2631 [7,8] it was found that the best kinetic model stemmed from a reaction mechanism in which the collaboration of an additional site is needed in the surface reaction. Adsorption of 2-propanol, isobutene, and IPTBE was assumed to be on one centre, since adsorption experiments with methanol and isobutene on zeolites by Kogelbauer et al. showed that a molecule of alcohol or olefin is adsorbed per acid site [27]. By assuming each step of the mechanisms as the rate-limiting step, we obtained the rate equations listed in Table 7. As the alcohol-olefin-ether system is nonideal, the concentration of the reacting species is given in activities. Activity coefficients were computed by the UNIFAC method.

To obtain the best model for the reaction, kinetic analysis began by a consideration of initial reaction rate data. The best kinetic model should describe appropriately the surface response of the reaction rate as a function of activities. As Table 8 shows, r^0_{IPTBE} decreases with increasing $R_{A/O}$, that is, with increasing 2-propanol activity, a_{IPA}, or decreasing isobutene activity, a_{IB}. Furthermore, since there is no reaction in the absence of alcohol, the appropriate model should predict a reaction rate maximum as a function of a_{IPA}. That is to say, the first derivative of the reaction rate with respect to a_{IB} has to be positive, whereas the second derivative of the reaction rate with respect a_{IPA} has to be negative.

At the beginning of the reaction there is no IPTBE in the reaction medium. Therefore, $a_{IPTBE} = 0$, and, as a consequence, the models of Table 7 can be simplified by neglecting the terms containing a_{IPTBE}. Simplified models that do not fulfill the surface response trends were discarded, and we fitted the rest by minimizing the sum of squares of lack

Table 7
Kinetic models tested to represent rate data of IPTBE synthesis

Mechanism	Rate-limiting step	Kinetic model	Equation
ER	2-Propanol adsorption	$r_{\mathrm{IPTBE}} = \dfrac{k_{\mathrm{IPA}}(a_{\mathrm{IPA}} - a_{\mathrm{IPTBE}}/K_{\mathrm{eq}}a_{\mathrm{IB}})}{1 + K_{\mathrm{IPA}}a_{\mathrm{IPA}}/Ka_{\mathrm{IB}} + K_{\mathrm{IPTBE}}a_{\mathrm{IPTBE}}}$	A
	Surface reaction	$r_{\mathrm{IPTBE}} = \dfrac{k_{\mathrm{S}}K_{\mathrm{IPA}}(a_{\mathrm{IB}}a_{\mathrm{IPA}} - a_{\mathrm{IPTBE}}/K_{\mathrm{eq}})}{1 + K_{\mathrm{IB}}a_{\mathrm{IB}} + K_{\mathrm{IPA}}a_{\mathrm{IPA}} + K_{\mathrm{IPTBE}}a_{\mathrm{IPTBE}}}$	B
	IPTBE desorption	$r = \dfrac{k_{\mathrm{IPTBE}}K(a_{\mathrm{IB}}a_{\mathrm{IPA}} - a_{\mathrm{IPTBE}}/K_{\mathrm{eq}})}{1 + K_{\mathrm{IPA}}a_{\mathrm{IPA}} + KK_{\mathrm{IPTBE}}a_{\mathrm{IPA}}a_{\mathrm{IB}}}$	C
LHHW	2-Propanol adsorption	$r_{\mathrm{IPTBE}} = \dfrac{k_{\mathrm{IPA}}(a_{\mathrm{IPA}} - a_{\mathrm{IPTBE}}/K_{\mathrm{eq}}a_{\mathrm{IB}})}{1 + K_{\mathrm{IPA}}a_{\mathrm{IPA}}/Ka_{\mathrm{IB}} + K_{\mathrm{IB}}a_{\mathrm{IB}} + K_{\mathrm{IPTBE}}a_{\mathrm{IPTBE}}}$	D
	Isobutene adsorption	$r_{\mathrm{IPTBE}} = \dfrac{k_{\mathrm{IB}}(a_{\mathrm{IB}} - a_{\mathrm{IPTBE}}/K_{\mathrm{eq}}a_{\mathrm{IPA}})}{1 + K_{\mathrm{IB}}a_{\mathrm{IB}}/Ka_{\mathrm{IPA}} + K_{\mathrm{IPA}}a_{\mathrm{IPA}} + K_{\mathrm{IPTBE}}a_{\mathrm{IPTBE}}}$	E
	Surface reaction	$r_{\mathrm{IPTBE}} = \dfrac{k_{\mathrm{S}}K_{\mathrm{IB}}K_{\mathrm{IPA}}(a_{\mathrm{IB}}a_{\mathrm{IPA}} - a_{\mathrm{IPTBE}}/K_{\mathrm{eq}})}{(1 + K_{\mathrm{IB}}a_{\mathrm{IB}} + K_{\mathrm{IPA}}a_{\mathrm{IPA}} + K_{\mathrm{IPTBE}}a_{\mathrm{IPTBE}})^2}$	F
	IPTBE desorption	$r_{\mathrm{IPTBE}} = \dfrac{k_{\mathrm{E}}K(a_{\mathrm{IB}}a_{\mathrm{IPA}} - a_{\mathrm{IPTBE}}/K_{\mathrm{eq}})}{1 + K_{\mathrm{IB}}a_{\mathrm{IB}} + K_{\mathrm{IPA}}a_{\mathrm{IPA}} + KK_{\mathrm{IPTBE}}a_{\mathrm{IPA}}a_{\mathrm{IB}}}$	G
LHHW [a]	Surface reaction	$r_{\mathrm{IPTBE}} = \dfrac{k_{\mathrm{S}}K_{\mathrm{IB}}K_{\mathrm{IPA}}(a_{\mathrm{IB}}a_{\mathrm{IPA}} - a_{\mathrm{IPTBE}}/K_{\mathrm{eq}})}{(1 + K_{\mathrm{IB}}a_{\mathrm{IB}} + K_{\mathrm{IPA}}a_{\mathrm{IPA}} + K_{\mathrm{IPTBE}}a_{\mathrm{IPTBE}})^3}$	H

[a] With the participation of an additional site in surface reaction.

Table 8
Initial reaction rates and activities of isobutene and 2-propanol

T (°C)	$R_{\mathrm{A/O}}$	a^0_{IB}	a^0_{IPA}	r^0_{IPTBE} (mol g^{-1} min^{-1})
69.2	0.7	0.8027	0.6024	0.0141
	1.0	0.7572	0.6458	0.0116
	2.0	0.6242	0.7389	0.0102
79.4	0.7	0.7958	0.5987	0.0299
	1.0	0.7494	0.6432	0.0279
	2.0	0.6157	0.7378	0.0199
89.5	0.7	0.7893	0.5951	0.0549
	1.0	0.7419	0.6408	0.0443
	2.0	0.6075	0.7367	0.0383

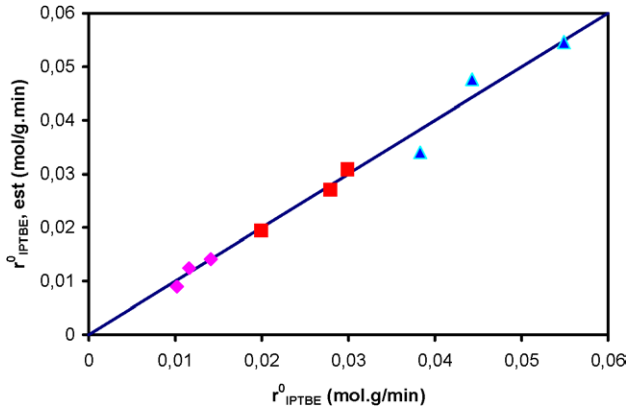

Fig. 6. Initial reaction rates estimated by model E2 vs. experimental ones (69.2 °C, ◆; 79.4 °C, ■; 89.5 °C, ▲).

of fit (SSQ). Models of Table 9 show the lower SSQ and, in addition, are thermodynamically coherent. They have one or two parameters to fit: products of rate constant and/or adsorption equilibrium constants of compounds. Models with three parameters were not thermodynamically coherent. It should be noted that all of the models of Table 9 stem from the LHHW mechanism. Models E1 and E2 assume olefin adsorption as the rate-limiting step, whereas F1, F2, F3, H1, and H2 assume that it is surface reaction. Fig. 6 shows that initial reaction rates predicted by model E2 agree well with the experimental data, which were the same as those for the other models of Table 9. The SSQ for all the models is very similar, and thus none of them were discarded at this stage of the screening process.

3.4. Integral kinetic study

To screen the best kinetic model it is necessary to explore the effect of a_{IPTBE} on the reaction rate. In batch experiments, the reaction rate decreases with time because of the formation of IPTBE, and it is zero at chemical equilibrium. So, the reaction rate decreases with increasing a_{IPTBE}. Kinetically, IPTBE reduces the driving force, and it could increase the adsorption term of models. In the integral study, equations of Table 10 were considered. They stem from the models of Table 9. A designates equations including a_{IPTBE} in the driving force, and B designates the models taking into account a_{IPTBE} in the adsorption term as well. Kinetic models of Table 10 contain a parameter to fit (models E2A and F3A), or two (E1A, F1A, F2A, E2B, F3B, H1A, and H2A), or three (E1B, F1B, F2B, H1B, and H2B). Such parameters are the apparent rate constant $\hat{k}$ and a combination of adsorption equilibrium constants.

To discriminate between kinetic models and to obtain simultaneously their parameter values, experimental data for X_{IB} versus time were fitted by numerical integration of the

Table 9
Kinetic models that represent initial reaction rate data appropriately ($a_{\mathrm{IPTBE}} = 0$)

Simplified kinetic model	Equation	Hypothesis	SSQ
$r_{\mathrm{IPTBE}} = \dfrac{(k_{\mathrm{IB}}K_{\mathrm{eq}}/K_{\mathrm{IB}})a_{\mathrm{IB}}a_{\mathrm{IPA}}}{a_{\mathrm{IB}} + (K_{\mathrm{IPA}}K_{\mathrm{eq}}/K_{\mathrm{IB}})a_{\mathrm{IPA}}^2}$	E1	$1 \ll \dfrac{K_{\mathrm{IB}}a_{\mathrm{IB}}}{K_{\mathrm{eq}}a_{\mathrm{IPA}}} + K_{\mathrm{IPA}}a_{\mathrm{IPA}}$	2.28×10^{-5}
$r_{\mathrm{IPTBE}} = \dfrac{(k_{\mathrm{S}}K_{\mathrm{IPA}}/K_{\mathrm{IB}})a_{\mathrm{IB}}a_{\mathrm{IPA}}}{(a_{\mathrm{IB}} + (K_{\mathrm{IPA}}/K_{\mathrm{IB}})a_{\mathrm{IPA}})^2}$	F1	$1 \ll K_{\mathrm{IB}}a_{\mathrm{IB}} + K_{\mathrm{IPA}}a_{\mathrm{IPA}}$	2.12×10^{-5}
$r_{\mathrm{IPTBE}} = \dfrac{k_{\mathrm{S}}K_{\mathrm{IB}}K_{\mathrm{IPA}}a_{\mathrm{IB}}a_{\mathrm{IPA}}}{(1 + K_{\mathrm{IPA}}a_{\mathrm{IPA}})^2}$	F2	$K_{\mathrm{IB}}a_{\mathrm{IB}} \ll 1 + K_{\mathrm{IPA}}a_{\mathrm{IPA}}$	2.35×10^{-5}
$r_{\mathrm{IPTBE}} = \dfrac{k_{\mathrm{IB}}a_{\mathrm{IB}}}{K_{\mathrm{IPA}}a_{\mathrm{IPA}}}$	E2	$1 + \dfrac{K_{\mathrm{IB}}a_{\mathrm{IB}}}{K_{\mathrm{eq}}a_{\mathrm{IPA}}} \ll K_{\mathrm{IPA}}a_{\mathrm{IPA}}$	3.40×10^{-5}
$r_{\mathrm{IPTBE}} = \dfrac{k_{\mathrm{S}}K_{\mathrm{IB}}a_{\mathrm{IB}}}{K_{\mathrm{IPA}}a_{\mathrm{IPA}}}$	F3	$1 + K_{\mathrm{IB}}a_{\mathrm{IB}} \ll K_{\mathrm{IPA}}a_{\mathrm{IPA}}$	3.40×10^{-5}
$r_{\mathrm{IPTBE}} = \dfrac{(k_{\mathrm{S}}K_{\mathrm{IPA}}/K_{\mathrm{IB}})a_{\mathrm{IB}}a_{\mathrm{IPA}}}{(a_{\mathrm{IB}} + (K_{\mathrm{IPA}}/K_{\mathrm{IB}})a_{\mathrm{IPA}})^3}$	H1	$1 \ll K_{\mathrm{IB}}a_{\mathrm{IB}} + K_{\mathrm{IPA}}a_{\mathrm{IPA}}$	1.96×10^{-5}
$r_{\mathrm{IPTBE}} = \dfrac{k_{\mathrm{S}}K_{\mathrm{IB}}K_{\mathrm{IPA}}a_{\mathrm{IB}}a_{\mathrm{IPA}}}{(1 + K_{\mathrm{IPA}}a_{\mathrm{IPA}})^3}$	H2	$K_{\mathrm{IB}}a_{\mathrm{IB}} \ll 1 + K_{\mathrm{IPA}}a_{\mathrm{IPA}}$	2.37×10^{-5}

equation

$$\frac{\mathrm{d}X_{\mathrm{IB}}}{\mathrm{d}t} = \frac{W}{n_{\mathrm{IB}}^0} r_{\mathrm{IPTBE}}, \tag{5}$$

where r_{IPTBE} is given by kinetic models of Table 10. Integration of Eq. (5) is performed by a fourth-order Runge–Kutta method, and the minimisation of the sum of squares of lack of fit between the experimental curves and the estimated values by integration was carried out by the Levenberg–Marquardt method [47]. The objective function was

$$\mathrm{SSQ} = \sum_{\text{All expts}} \left(\sum_{n_j} (X_{\mathrm{IB,exp}} - X_{\mathrm{IB,est}})^2 \right). \tag{6}$$

Since rate constant and adsorption equilibrium constants are exponential functions of reciprocal absolute temperature, the temperature dependence of parameters was considered to fulfill the following relationship:

$$\hat{k} = \exp(b_1) \exp\left[b_2 \left(\frac{1}{T} - \frac{1}{\overline{T}} \right) \right], \tag{7}$$

$$K[j] = \exp(d_1) \exp\left[d_2 \left(\frac{1}{T} - \frac{1}{\overline{T}} \right) \right]. \tag{8}$$

The fitted parameters are represented by b and d. The exponential form of the first factor and the subtraction of the reciprocal of the mean experimental temperature were included in Eqs. (7) and (8) to obtain the lowest correlation between fitted parameters. The chemical equilibrium constant, K_{eq}, was computed by [3]

$$\ln K_{\mathrm{eq}} = -500.965 + \frac{10599.2}{T} + 100.038 \ln T - 0.466235T + 4.944111 \times 10^{-4}T^2 - 2.83523 \times 10^{-7}T^3. \tag{9}$$

Ideally, from a mathematical point of view, the most suitable model is the one with the least SSQ, the fewest random residuals, and low parameter correlation. Furthermore, fitted parameters should have physicochemical meaning: the rate constant should increase when the temperature increases, and adsorption equilibrium constants should decrease. As a result, activation energy should be positive, and adsorption enthalpies and entropies should be negative.

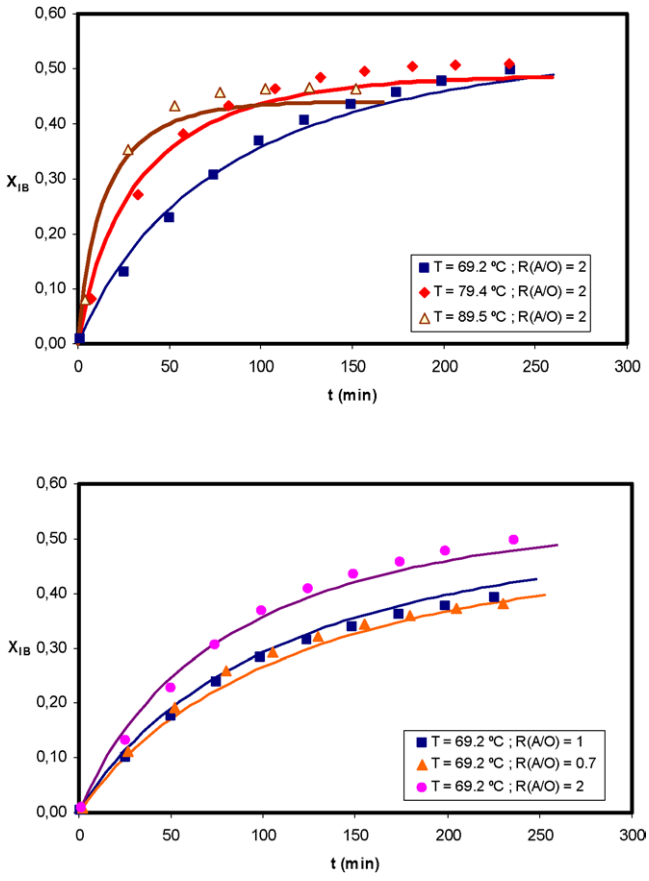

Fig. 7. IB conversion estimated by model F3B (solid lines) and experimental data at different temperatures and $R_{\mathrm{A/O}}$.

Table 10
Kinetic models fitted in the integral study

Equation	Kinetic model	Fitted parameters	SSQ	Remarks of the fit
E1A	$r_{\mathrm{IPTBE}} = \dfrac{\hat{k}(a_{\mathrm{IB}} - a_{\mathrm{IPTBE}}/K_{\mathrm{eq}}a_{\mathrm{IPA}})}{(a_{\mathrm{IB}}/a_{\mathrm{IPA}}) + K[1]a_{\mathrm{IPA}}}$	$\hat{k} = k_{\mathrm{IB}}K_{\mathrm{eq}}/K_{\mathrm{IB}}$ $K[1] = K_{\mathrm{IPA}}K_{\mathrm{eq}}/K_{\mathrm{IB}}$	0.106	TC
E1B	$r_{\mathrm{IPTBE}} = \dfrac{\hat{k}(a_{\mathrm{IB}} - a_{\mathrm{IPTBE}}/K_{\mathrm{eq}}a_{\mathrm{IPA}})}{(a_{\mathrm{IB}}/a_{\mathrm{IPA}}) + K[1]a_{\mathrm{IPA}} + K[2]a_{\mathrm{IPTBE}}}$	$\hat{k} = k_{\mathrm{IB}}K_{\mathrm{eq}}/K_{\mathrm{IB}}$ $K[1] = K_{\mathrm{IPA}}K_{\mathrm{eq}}/K_{\mathrm{IB}}$ $K[2] = K_{\mathrm{IPTBE}}K_{\mathrm{eq}}/K_{\mathrm{IB}}$	0.046	TC TMIC
F1A	$r_{\mathrm{IPTBE}} = \dfrac{\hat{k}(a_{\mathrm{IB}}a_{\mathrm{IPA}} - a_{\mathrm{IPTBE}}/K_{\mathrm{eq}})}{(a_{\mathrm{IB}} + K[1]a_{\mathrm{IPA}})^2}$	$\hat{k} = k_{\mathrm{S}}K_{\mathrm{IPA}}/K_{\mathrm{IB}}$ $K[1] = K_{\mathrm{IPA}}/K_{\mathrm{IB}}$	0.116	TC
F1B	$r_{\mathrm{IPTBE}} = \dfrac{\hat{k}(a_{\mathrm{IB}}a_{\mathrm{IPA}} - a_{\mathrm{IPTBE}}/K_{\mathrm{eq}})}{(a_{\mathrm{IB}} + K[1]a_{\mathrm{IPA}} + K[2]a_{\mathrm{IPTBE}})^2}$	$\hat{k} = k_{\mathrm{S}}K_{\mathrm{IPA}}/K_{\mathrm{IB}}$ $K[1] = K_{\mathrm{IPA}}/K_{\mathrm{IB}}$ $K[2] = K_{\mathrm{IPTBE}}/K_{\mathrm{IB}}$	0.0385	TC TMIC
F2A	$r_{\mathrm{IPTBE}} = \dfrac{\hat{k}(a_{\mathrm{IB}}a_{\mathrm{IPA}} - a_{\mathrm{IPTBE}}/K_{\mathrm{eq}})}{(1 + K[1]a_{\mathrm{IPA}})^2}$	$\hat{k} = k_{\mathrm{S}}K_{\mathrm{IPA}}K_{\mathrm{IB}}$ $K[1] = K_{\mathrm{IPA}}$	0.079	TC TMIC
F2B	$r_{\mathrm{IPTBE}} = \dfrac{\hat{k}(a_{\mathrm{IB}}a_{\mathrm{IPA}} - a_{\mathrm{IPTBE}}/K_{\mathrm{eq}})}{(1 + K[1]a_{\mathrm{IPA}} + K[2]a_{\mathrm{IPTBE}})^2}$	$\hat{k} = k_{\mathrm{S}}K_{\mathrm{IPA}}K_{\mathrm{IB}}$ $K[1] = K_{\mathrm{IPA}}$ $K[2] = K_{\mathrm{IPTBE}}$	0.038	No TC
E2A	$r_{\mathrm{IPTBE}} = \dfrac{\hat{k}(a_{\mathrm{IB}} - a_{\mathrm{IPTBE}}/K_{\mathrm{eq}}a_{\mathrm{IPA}})}{a_{\mathrm{IPA}}}$	$\hat{k} = k_{\mathrm{IB}}/K_{\mathrm{IPA}}$	0.139	TC
E2B	$r_{\mathrm{IPTBE}} = \dfrac{\hat{k}(a_{\mathrm{IB}} - a_{\mathrm{IPTBE}}/K_{\mathrm{eq}}a_{\mathrm{IPA}})}{a_{\mathrm{IPA}} + K[1]a_{\mathrm{IPTBE}}}$	$\hat{k} = k_{\mathrm{IB}}/K_{\mathrm{IPA}}$ $K[1] = K_{\mathrm{IPTBE}}/K_{\mathrm{IPA}}$	0.066	TC
F3A	$r_{\mathrm{IPTBE}} = \dfrac{\hat{k}(a_{\mathrm{IB}}a_{\mathrm{IPA}} - a_{\mathrm{IPTBE}}/K_{\mathrm{eq}})}{a_{\mathrm{IPA}}^2}$	$\hat{k} = k_{\mathrm{S}}K_{\mathrm{IB}}/K_{\mathrm{IPA}}$	0.137	TC
F3B	$r_{\mathrm{IPTBE}} = \dfrac{\hat{k}(a_{\mathrm{IB}}a_{\mathrm{IPA}} - a_{\mathrm{IPTBE}}/K_{\mathrm{eq}})}{(a_{\mathrm{IPA}} + K[1]a_{\mathrm{IPTBE}})^2}$	$\hat{k} = k_{\mathrm{S}}K_{\mathrm{IB}}/K_{\mathrm{IPA}}$ $K[1] = K_{\mathrm{IPTBE}}/K_{\mathrm{IPA}}$	0.060	TC
H1A	$r_{\mathrm{IPTBE}} = \dfrac{\hat{k}(a_{\mathrm{IB}}a_{\mathrm{IPA}} - a_{\mathrm{IPTBE}}/K_{\mathrm{eq}})}{(a_{\mathrm{IB}} + K[1]a_{\mathrm{IPA}})^3}$	$\hat{k} = k_{\mathrm{S}}K_{\mathrm{IB}}/K_{\mathrm{IPA}}^2$ $K[1] = K_{\mathrm{IPA}}/K_{\mathrm{IB}}$	0.143	TC TMIC
H1B	$r_{\mathrm{IPTBE}} = \dfrac{\hat{k}(a_{\mathrm{IB}}a_{\mathrm{IPA}} - a_{\mathrm{IPTBE}}/K_{\mathrm{eq}})}{(a_{\mathrm{IB}} + K[1]a_{\mathrm{IPA}} + K[2]a_{\mathrm{IPTBE}})^3}$	$\hat{k} = k_{\mathrm{S}}K_{\mathrm{IB}}/K_{\mathrm{IPA}}^2$ $K[1] = K_{\mathrm{IPA}}/K_{\mathrm{IB}}$ $K[2] = K_{\mathrm{IPTBE}}/K_{\mathrm{IB}}$	0.038	No TC TMIC
H2A	$r_{\mathrm{IPTBE}} = \dfrac{\hat{k}(a_{\mathrm{IB}}a_{\mathrm{IPA}} - a_{\mathrm{IPTBE}}/K_{\mathrm{eq}})}{(1 + K[1]a_{\mathrm{IPA}})^3}$	$\hat{k} = k_{\mathrm{S}}K_{\mathrm{IB}}K_{\mathrm{IPA}}$ $K[1] = K_{\mathrm{IPA}}$	0.075	TC TMIC
H2B	$r_{\mathrm{IPTBE}} = \dfrac{\hat{k}(a_{\mathrm{IB}}a_{\mathrm{IPA}} - a_{\mathrm{IPTBE}}/K_{\mathrm{eq}})}{(1 + K[1]a_{\mathrm{IPA}} + K[2]a_{\mathrm{IPTBE}})^3}$	$\hat{k} = k_{\mathrm{S}}K_{\mathrm{IB}}K_{\mathrm{IPA}}$ $K[1] = K_{\mathrm{IPA}}$ $K[2] = K_{\mathrm{IPTBE}}$	0.075	No TC TMIC

TC, thermodynamically coherent; TMIC, two many iteration cycles.

Models E1B, F1B, F2A, H1A, H1B, H2A, and H2B hardly converge (Table 10), and the iteration process stopped when the maximum number fixed by the fitting procedure was reached. They were therefore discarded. On the other hand, model F2B was discarded because it is not thermodynamically coherent. Of the other models, F3B and E2B represent data much better. Fig. 7 shows a plot of estimated values against experimental values for model F3B. Taking into account that parameter values were obtained by the simultaneous fit of all of the experimental curves, we can conclude that the fit is satisfactory.

To screen between models F3B and E2B, we fitted them again by considering K_{eq} as a parameter to fit as well. New parameter values are compared with those found in the previous fit in Table 11. For model F3B, $\hat{k}$ estimates are nearly the same at each temperature; those of $K[1]$ agree at 69.2 °C, but they are less sensitive to temperature in the new fit, probably because of the high correlation between parameters; finally, K_{eq} values agree very well with those computed with Eq. (9). From the variation of K_{eq} estimates with temperature, a reaction enthalpy of $-26.7\ \mathrm{kJ\,mol^{-1}}$ was computed, which coincides within the limits of the experimental error with the value of $-25.9 \pm 1.3\ \mathrm{kJ\,mol^{-1}}$ found from chemical equilibrium experiments in the temperature range explored [3].

As for model E2B, estimates of $\hat{k}$, and particularly of $K[1]$, are quite different from those found in the fit with the use of K_{eq} values from Eq. (9). Estimates of K_{eq} agree poorly with the thermodynamic values. Finally, from the temperature dependence of K_{eq} estimates, a reaction en-

Table 11
Comparison between parameter values of models E2B and F3B

	Fit using K_{eq} computed by Eq. (10)		Fit including K_{eq}			
T (°C)	$\hat{k}$ (mol g^{-1} min^{-1})	K[1]	$\hat{k}$ (mol g^{-1} min^{-1})	K_{eq}	K[1]	K_{eq} by Eq. (10)
			Model F3B			
69.2	0.0177	1.749	0.0189	2.072	1.754	2.050
79.4	0.0450	2.197	0.0459	1.578	2.016	1.596
89.5	0.109	2.725	0.106	1.220	2.298	1.260
			Model E2B			
69.2	0.0198	5.46	0.0171	1.866	3.67	2.050
79.4	0.0485	6.78	0.0396	1.477	3.64	1.596
89.5	0.113	8.31	0.0871	1.185	3.62	1.260

thalpy of -22.9 kJ mol^{-1} was found, which does not agree within the limits of the experimental error with the value of -25.9 ± 1.3 kJ mol^{-1} computed from equilibrium experiments [3].

Ideally, kinetic estimates of K_{eq} should be the same as values found from equilibrium experiments. Therefore, we conclude that the best kinetic model for IPTBE synthesis is F3B

$$r_{IPTBE} = \frac{\hat{k}(a_{IB}a_{IPA} - a_{IPTBE}/K_{eq})}{(a_{IPA} + K[1]a_{IPTBE})^2}. \quad (10)$$

The apparent rate constant, $\hat{k}$, and the quotient of adsorption equilibrium constants, K[1], are, respectively,

$$\hat{k} = \frac{k_S K_{IB}}{K_{IPA}} = \exp(-3.043 \pm 0.090) \times \exp\left[(-11040 \pm 1430)\left(\frac{1}{T} - \frac{1}{353.15}\right)\right], \quad (11)$$

$$K[1] = \frac{K_{IPTBE}}{K_{IPA}} = \exp(0.801 \pm 0.138) \times \exp\left[(-2697 \pm 2035)\left(\frac{1}{T} - \frac{1}{353.15}\right)\right]. \quad (12)$$

From the temperature dependence of $\hat{k}$, an apparent activation energy, E_{app}, of 92 ± 12 kJ mol^{-1} was computed. Moreover, from the temperature dependence of K[1] it was found that the adsorption enthalpy of 2-propanol is higher than that of IPTBE, and their relation is

$$\Delta\widehat{H}_{a,IPA} = \Delta\widehat{H}_{a,IPTBE} - 22.4 \text{ kJ mol}^{-1}. \quad (13)$$

Model F3B stems from a mechanism wherein 2-propanol and isobutene adsorbed on one site react to give the ether, surface reaction is the rate-controlling step, and adsorption of 2-propanol and IPTBE is significant. In kinetic studies on ion exchangers, it is seen that the best model is a similar one, but three active sites take part in the rate-controlling step [5,7,8]. The different kinetic behaviour is due to the fact that having three active sites close enough and, at the same time, accessible to reactants is more difficult on H-Beta. Its acid capacity is a quarter of that of commercial resins (Table 1), and its surface area (external and pores) is far higher than that of swollen resins (typically, 160–200 m^2 g^{-1} [48]). So, the surface concentration of active sites is lower on H-Beta. Moreover, the surface of resins swollen in the presence of polar compounds such as alcohols is made up by flexible polymer chains, so that it is possible to accommodate the reaction intermediate on three acidic sites, unlike on the crystalline surface of H-Beta.

Table 12
Apparent activation energies for IPTBE synthesis on H-Beta and on ion-exchangers

Catalyst	E_{app} (kJ mol^{-1})	Type of kinetic study	Reference
Bayer K2631	70.3–78.4	Data obtained in calorimetric reactor	[5]
	75.5	Integral study. Data obtained in batch rector	[7]
Amberlyst 15	68–72	Study based on initial reaction rates. Data obtained in batch rector	[8]
Amberlyst 35			
H-Beta	92 ± 12	Integral study. Data obtained in batch rector	This work

The apparent activation energy is a bit higher that those found on ion exchangers, as Table 12 shows, in agreement with the experimental fact that, in general, resins are more active in synthesising *tert*-alkyl ethers from alcohol and isobutene.

4. Conclusions

The addition of 2-propanol to isobutene to yield IPTBE has been studied in the liquid phase on H-Beta, H-Y, and H-ZSM-5. The SiO_2/Al_2O_3 ratio was about 25 for H-Beta, 6 for H-Y, and 28 for H-ZSM-5, respectively. First, their activation conditions were optimised, and from the activity and selectivity of zeolites it was concluded that the best activation conditions are as follows: H-ZSM-5, calcination at 200–300 °C for 2–4 h; H-Y, 500 °C for 2–4 h; and H-Beta, 405–440 °C for 2–4 h. Second, by comparing the selectivity and activity of zeolites activated under optimal conditions, it is seen that H-Beta gives the best results, being as active as commercial ion-exchange resins, but a bit less selective. Finally, the kinetic study of IPTBE synthesis over H-Beta shows that the best kinetic model stems from a mechanism

in which isobutene reacts with 2-propanol, both of two adsorbed on one site, giving rise to the ether adsorbed on one site. The apparent activation energy was estimated to be $92 \pm 12\ \mathrm{kJ\,mol^{-1}}$.

Nomenclature

a_j	Activity of compound j, dimensionless;
$c_{\mathrm{IPA,S}}$	Concentration of 2-propanol at the external surface, $\mathrm{mol\,l^{-1}}$;
E_{app}	Apparent activation energy, $\mathrm{kJ\,mol^{-1}}$;
$D_{\mathrm{e,IPA}}$	Effective diffusivity of 2-propanol, $\mathrm{m^2\,s^{-1}}$;
$\bar{d}_{\mathrm{pore}}$	Mean mesopore diameter, nm;
k_j	Rate constant of adsorption of compound j, $\mathrm{mol\,min^{-1}\,g^{-1}}$;
k_s	Rate constant of reaction surface, $\mathrm{mol\,min^{-1}\,g^{-1}}$;
K_{eq}	Thermodynamic equilibrium constant, dimensionless;
K_j	Adsorption equilibrium constant of compound j, dimensionless;
L_{e}	Effective diffusion-path-length parameter, m;
$\overline{M}$	Molecular weight, $\mathrm{g\,mol^{-1}}$;
n_j	Mole number of compound j, mol;
r_{IPTBE}	Reaction rate of IPTBE synthesis on a dry-weight catalyst basis, $\mathrm{mol\,min^{-1}\,g^{-1}}$;
$R_{\mathrm{A/O}}$	Initial 2-propanol/isobutene molar ratio;
SSQ	Sum of squares of lack of fit;
S_{ext}	External surface area, $\mathrm{m^2\,g^{-1}}$;
S_{g}	BET surface area, $\mathrm{m^2\,g^{-1}}$;
S_{meso}	Surface area of meso and macropores, $\mathrm{m^2\,g^{-1}}$;
S	Selectivity;
T_{c}	Calcination temperature, °C;
$\overline{T}$	Mean temperature, K;
t_{c}	Calcination time, h;
t	Time, min or h;
V_{g}	Total pore volume, $\mathrm{cm^3\,g^{-1}}$;
V_{meso}	Pore volume relative to meso- and macropores, $\mathrm{cm^3\,g^{-1}}$;
V_{μ}	Pore volume relative to micropores, $\mathrm{cm^3\,g^{-1}}$;
W	Catalyst mass, g;
X_{IB}	Equilibrium conversion of IB;
Y	Yield;
Φ	Weisz–Prater modulus, dimensionless;
$\Delta\widehat{H}_{\mathrm{a},j}$	Adsorption enthalpy of compound j, $\mathrm{kJ\,mol^{-1}}$;
δ	Molecular random coil, Å;
θ	Porosity;
ρ_{s}	Skeletal density, $\mathrm{g\,cm^{-3}}$;
ρ_{P}	Particle density, $\mathrm{g\,cm^{-3}}$;
σ	Active site.

Superscripts and subscripts

DIPE	Diisopropyl ether;
IB	Isobutene;
IPA	2-Propanol;
IPTBE	Isopropyl *tert*-butyl ether;
0	Initial ($t = 0$);
TBA	*tert*-Butyl alcohol;
TMP-1	2,4,4-trimethyl-1-pentene;
TMP-2	2,4,4-trymethyl-2-pentene.

References

[1] G.H. Unzelman, Fuel Reformulation 2 (6) (1992) 34–40.
[2] M.N. Harandi, H. Owen, US Patent 5,011,506 (1991), to Mobil Oil Corporation.
[3] A. Calderón, J. Tejero, J.F. Izquierdo, M. Iborra, F. Cunill, Ind. Eng. Chem. Res. 36 (1997) 896.
[4] J. Tejero, A. Calderón, F. Cunill, J.F. Izquierdo, M. Iborra, React. Funct. Polym. 33 (1997) 201.
[5] L. Solá, M.A. Pericàs, F. Cunill, J.F. Izquierdo, Ind. Eng. Chem. Res. 36 (1997) 2012.
[6] J.A. Linnekoski, A.O.I. Krause, A. Holmen, M. Kjesta, K. Moljord, Appl. Catal. A 174 (1998) 1.
[7] F. Cunill, M. Iborra, C. Fité, J. Tejero, J.F. Izquierdo, Ind. Eng. Chem. Res. 39 (2000) 1235.
[8] J. Tejero, E. Creus, M. Iborra, F. Cunill, J.F. Izquierdo, C. Fité, Catal. Today 65 (2001) 381.
[9] J.G. Goodwin Jr., S. Natesakhawat, A.A. Nikolopoulos, S.Y. Kim, Catal. Rev. 44 (2) (2002) 287.
[10] F. Collignon, M. Mariani, S. Moreno, M. Remy, G. Poncelet, J. Catal. 166 (1997) 53.
[11] F. Collignon, G. Poncelet, J. Catal. 202 (2001) 68.
[12] F. Collignon, R. Loenders, J.A. Martens, P.A. Jacobs, G. Poncelet, J. Catal. 182 (1999) 302.
[13] P. Chu, G.H. Kühl, Ind. Eng. Chem. Res. 26 (1987) 365.
[14] S.I. Pien, W.J. Hatcher, Chem. Eng. Commun. 93 (1990) 257.
[15] M.A. Ali, B.J. Brisdon, W.J. Thomas, Appl. Catal. A 197 (2000) 303.
[16] M.A. Ali, B.J. Brisdon, W.J. Thomas, Appl. Catal. A 252 (2003) 149.
[17] L.M. Tau, B.H. Davis, Appl. Catal. 53 (1989) 263.
[18] A.A. Nikolopoulos, A. Kogelbauer, J.G. Goodwin Jr., G. Marcelin, Appl. Catal. 119 (1994) 69.
[19] A.J. Lecloux, in: J.R. Anderson, M. Boudart (Eds.), in: Catalysis Science and Technology, vol. 2, Springer, Berlin, 1981, p. 171.
[20] M.J. Remy, G.A. Poncelet, J. Phys. Chem. 99 (1995) 773.
[21] E.P. Barret, L.G. Joyner, P.P. Halenda, J. Am. Chem. Soc. 73 (1951) 373.
[22] R. Szostack, in: Handbook of Molecular Sieves, Van Nostrand Reinhold, New York, 1992, pp. 93, 183 and 518.
[23] J.F. Izquierdo, F. Cunill, M. Vila, J. Tejero, M. Iborra, J. Chem. Eng. Data 37 (1992) 339.
[24] R.W. Missen, Ch.A. Mims, B.A. Saville, in: Introduction to Chemical Reaction Engineering and Kinetics, Wiley, New York, 1999, p. 92.
[25] C.N. Satterfield, in: Heterogeneous Catalysis in Practice, McGraw–Hill, New York, 1991, p. 12.
[26] S.H. Ahmed, M.Z. El-Faer, M.M. Abdillahi, M.A.B. Siddiqui, S.A.I. Barri, Arabian J. Sci. Eng. 21 (2) (1996) 283.
[27] S.H. Ahmed, M.Z. El-Faer, M.M. Abdillahi, J. Shirokoff, M.A.B. Siddiqui, S.A.I. Barri, Appl. Catal. A 161 (1997) 47.
[28] A. Kogelbauer, A.A. Nikolopoulos, J.G. Goodwin Jr., G. Marcelin, J. Catal. 152 (1995) 122.
[29] A. Kogelbauer, M. Öcal, A.A. Nikolopoulos, J.G. Goodwin Jr., G. Marcelin, J. Catal. 148 (1994) 157.
[30] R. LeVan Mao, T.S. Le, M. Fairbain, A. Muntasar, S. Xiao, G. Denes, Appl. Catal. A 185 (1991) 41.
[31] R. LeVan Mao, H. Ahlafi, T.S. Le, ACS Symp. Ser. 517 (1993) 233.
[32] A.A. Nikolopoulos, A. Kogelbauer, J.G. Goodwin Jr., G. Marcelin, J. Catal. 158 (1996) 76.
[33] A.A. Nikolopoulos, R. Oukaci, J.G. Goodwin Jr., G. Marcelin, Catal. Lett. 27 (1994) 149.

[34] A.A. Nikolopoulos, T.P. Palucka, P.V. Shertukde, R. Oukaci, J.G. Goodwin Jr., G. Marcelin, Stud. Surf. Sci. Catal. 74 (1993) 787.
[35] T. Rorvik, H. Mostad, O.H. Ellestad, M. Stöcker, Appl. Catal. A 137 (1996) 235.
[36] B.C. Gates, in: Catalytic Chemistry, Wiley, New York, 1992, p. 269.
[37] J.W. Ward, J. Catal. 11 (1968) 251.
[38] F. Asinger, in: Monoolefins Chemistry and Technology, Pergamon Press, Oxford, 1968, p. 963.
[39] R.L. Albright, React. Polym. 4 (1986) 155.
[40] M. Hunger, T. Horvath, Catal. Lett. 49 (1997) 95.
[41] A. Chakrabarti, M.M. Sharma, React. Polym. 20 (1993) 1.
[42] E. Creus, Ms. Chem. Eng. Thesis, University of Barcelona, 1998.
[43] J. Bo, Ms. Chem. Eng. Thesis, University of Barcelona, 1999.
[44] G.F. Froment, K.B. Bischoff, in: Chemical Reactor Analysis and Design, second ed., Wiley, New York, 1990, p. 167.
[45] R. Taylor, R. Krishna, in: Multicomponent Mass Transfer, Wiley, New York, 1993, p. 74.
[46] P.B. Weisz, CHEMTECH 3 (1973) 498.
[47] W.H. Press, S.A. Teukolsky, W.T. Vetterling, B.P. Flannerty, in: Numerical Recipes in C: The Art of Scientific Computing, second ed., Cambridge University Press, New York, 1992, p. 683.
[48] K. Jerabek, 2002, personal communication.